Acta Astronautica 121 (2016) 144–152

Contents lists available at ScienceDirect

Acta Astronautica

journal homepage: www.elsevier.com/locate/actaastro

Temperature-dependent emissivity property in $La_{0.7}Sr_{0.3}MnO_3$ films

Desong Fan *, Qiang Li, Ping Dai

School of Energy and Power Engineering, Nanjing University of Science and Technology, Nanjing, Jiangsu 210094, China

ARTICLE INFO

Article history:
Received 15 May 2015
Received in revised form
13 November 2015
Accepted 4 January 2016
Available online 12 January 2016

Keywords:
Thermochromic film
Variable emissivity
Thermal control

ABSTRACT

Thermochromic films have been deposited by magnetron sputtering technique on different substrates. The crystallinity and surface morphology of the films have been characterized. Characterization result shows that the films are of perovskite structure. Composition analysis is performed and the result indicated that the element composition of the film can be close to its stoichiometric ratio. Temperature-dependent reflectivity and emissivity are studied. Reflectivity spectra show a downward trend with increasing temperature. Emissivity of the film is large at high temperature and it decreases sharply upon cooling. The emissivity increment at 123–373 K can approach 0.43 at 1.4 Pa sputtering pressure environment, which is attractive for thermal control application in spacecraft.

1. Introduction

Thermochromic materials based on manganese oxides are very suitable for radiator application in space. They are characterised by tunable thermal radiative properties with the variation of their own temperature, as a result of a metal-insulator (MI) phase transition [1–3]. Since their emissivity is small at temperature below the phase transition temperature and large at higher temperature, emissivity adjustment can be achieved automatically by temperature control. If a radiator composed of thermochromic material is fitted on a spacecraft surface, the emissive heat transfer from spacecraft can be automatically controlled without additional power consumption and moving parts [4,5]. Thermochromic materials, therefore, attracted great attention in space thermal control application since the 1990s. Thermal radiative properties of the doped manganites $La_{1-x}A_xMnO_3$ (A is alkaline earth) have been deeply investigated since 1999 by Tachikawa et al. [6], who reported for the first time that a large emissivity variation for the thermochromic materials was observed in the Ca- or Sr-doped $LaMnO_3$ samples. Moreover, the emissivity of the material shows a drastically increase upon heating to a critical temperature called MI transition temperature T_{MI}.

Investigators have performed a series of explorations concerning the development of variable emissivity device based on the thermochromic materials in order to realize an attractive industrial application. These explorations involve the method of device fabrication, the evaluation of device thermal radiative properties (i.e., emissivity and solar absorptivity), and the stability of device in space environment. A ceramic tile device with sub-millimeter thickness was fabricated by machining and polishing the high-temperature sintered samples, which is the most employed fabrication method in present [2,5,7]. The investigation result of thermal radiative properties shows that a large emissivity variation ($\Delta\epsilon = 0.4$) for the device is comparable to that of the convectional thermal control louver, although it is imperfect to possess a high solar absorptivity about 0.8. In order to overcome the drawback of absorbing solar radiation and simultaneously hold the

* Corresponding author. Tel.: + 86 025 84315837.
E-mail address: dsfan@njust.edu.cn (D. Fan).

http://dx.doi.org/10.1016/j.actaastro.2016.01.001
0094-5765/

large emissivity variation, a spectral selective structure was designed on the device surface, and the solar absorptivity of the structured device was reduced to 0.28 [8–11]. The simulated experiment of space particles exposure revealed that the structured device possesses stable thermal radiative properties [3,12]. The applicability of the device have been demonstrated on the 'Hayabusa' spacecraft launched in 2003 by Japan Aerospace Exploration Agency [13]. It is reported that the device in 'Hayabusa' spacecraft reduces the energy consumption of the on-board heater, and decreases the weight and the cost of the thermal control system [14]. The groups of Xuan [15–18] from the standpoint of surface structures attempt to improve the tunable emissivity properties of thermochromic material. Huang et al. [15] calculated the spectral emissivity distribution of $La_{0.825}Sr_{0.175}MnO_3$ with one-dimensional grating structured surfaces using the finite difference time domain method. The results showed that the thermochromic performance of the material was improved by the structured surface, which have been demonstrated experimentally by means of photolithographic technique to construct a similar structured surface [16]. Then, by combining $La_{0.825}Sr_{0.175}MnO_3$ with Al and SiO_2 gratings, they theoretically enhanced the emissivity increment of the structure based on the near-field effect of thermal radiation [17,18].

In these previous works, a series of investigation efforts showed that thermochromic materials for space applications are very attractive due to their suitable thermal radiative properties and high radiation durability. However, the fabrication and application of the ceramic tile device is inconvenient and low productive because of its low toughness. In addition, it is also difficult to further lose weight by machining and polishing way in view of the weakened mechanical strength. By comparison, thin film devices based on thermochromic material may be more advantageous from the viewpoint of producibility. At present, several studies on the tunable emissivity properties of thermochromic film have been undertaken. Shimakawa et al. [19] investigated the dependence of the emissivity property on the thickness of thermochromic films (La,Sr)MnO_3, which were synthesized by a sol-gel method. Their results revealed that thermochromic film with the thickness of 1500 nm can be used for variable emissivity radiators. Thermal radiative properties of plasma sprayed thermochromic coating were reported that the coating with thickness 190 μm can be developed as variable emissivity coating [20]. Soltani et al. [21] and Nikanpour et al. [22] prepared the $La_{1-x}Sr_xMnO_3$ ($x=0.175$ and 0.3) thin films by reactive pulsed laser deposition method, but their emissivity variation remains modest. Wu et al. [23] prepared the $La_{0.8}Sr_{0.2}MnO_3$ thin film by magnetron sputtering, whose emissivity increases from 0.53 at 173 K to 0.72 at 310 K. Obviously, the emissivity variation of these thin films is still smaller than that of their bulk counterparts. Therefore, further investigation will be required to access the bulk material properties in emissivity as much as possible.

Thermochromic films that are fabricated on flexible substrates, such as PI substrate, will significantly broaden the applications and greatly reduce the material cost. However, it is extremely difficult to fabricate the films on flexible substrate because the thermal, chemical properties of the substrates are not compatible with the processes of high temperature used for preparing thermochromic film. For example, a melting temperature of PI material is less than 300 °C, which is far below the recrystallization temperatures 700 °C for thermochromic films. Recently, it was reported that a transfer printing method has been developed for flexible Si or GaAs film cells preparation without changing the cell material deposition conditions [24]. The process includes the film deposition onto rigid substrate with high temperature resistance, the film peeling-off from rigidness substrate, and the transfer printing of film. During the process, the film peeling-off from rigidness substrate relies on the phenomenon of water-assisted subcritical debonding at interface between metallic layer and rigidness substrate, which separates the metallic layer together with thin film cells from the original substrate [25]. As such, we expect that the method can be used to the peeling-off of thermochromic films. In present work, $La_{0.7}Sr_{0.3}MnO_3$ (LSMO) films were deposited on the Al coated quartz (ACQ) substrates at different sputtering pressure by a magnetron sputtering technique, and followed by annealing in oxygen atmosphere. The Al layer is used to as the metallic layer of transfer printing method. The structural, surface morphology, and thermochromic properties of the films have been investigated. The films grown on quartz, Si, and YSZ substrates were also presented to make a comparison.

2. Procedure for experiment

LSMO films were prepared on ACQ substrates by magnetron sputtering technique. The LSMO target used during sputtering was synthesized by the conventional solid-state reaction method using La_2O_3, $SrCO_3$ and MnO_2 powders as starting materials [5]. The LSMO films were grown in a mixed gas of argon with 20 vol% of oxygen and at different sputtering pressure P_{gas}. The substrate was kept at room temperature in view of instrument limit. After deposition, the as-grown films on ACQ substrate were annealed ex-situ at 873 K in flowing oxygen atmosphere for 2 h. In case of the films on Si, YSZ, and quartz substrates were sputtered in an oxygen flow ratio 20 vol% and a sputtering pressure 0.8 Pa and were annealed ex-situ at 1073 K for 1 h. Deposition conditions in experiment were listed in Table 1. The film structure was characterized by X-ray diffraction (XRD, D8, Bruker Co., Germany) with the Cu Kα ($\lambda=0.15406$ nm) radiation source at room temperature. Surface microstructure of the film was analyzed by field emission scanning electron microscopy (SEM, S-4800, Hitachi Co., Japan). Composition analysis was performed by the energy dispersive X-ray spectroscopy (EDS, Thermo Electron Co., USA). The thicknesses of several films were obtained from the cross-sectional SEM images, and the deposition rate Γ was estimated. Thus, the film thickness can be easily controlled by the sputtering time. LSMO film was characterized by X-ray photoelectron spectroscopy (XPS, PHI Quantera II, Ulvac-Phi Co., JPN). Surface roughness of the film was measured by the atomic force

Table 1
Deposition conditions of preparing LSMO films.

Film sample	Substrate	P_{gas} (Pa)	Γ (nm/min)
LSMOACQ05	ACQ	0.5	5.6
LSMOACQ08	ACQ	0.8	5.8
LSMOACQ14	ACQ	1.4	5.9
LSMOACQ20	ACQ	2.0	5.2
LSMOSi08	Si	0.8	4.9
LSMOYSZ08	YSZ	0.8	5.0

microscope (AFM, CSPM4000, Being Ltd., Beijing in China). The lateral resolution of the AFM is 0.26 nm and the vertical one is 0.1 nm. Infrared emissivity ϵ determining thermal radiative properties of film was derived from reflectivity spectra according to ECSS-Q-70-09 [26], as expressed by

$$\epsilon(T) = \frac{\int_{2.5}^{25}[1-\rho(\lambda,T)]E_{\lambda b}(\lambda,T)\,d\lambda}{\int_{2.5}^{25}E_{\lambda b}(\lambda,T)\,d\lambda}, \quad (1)$$

where $E_{\lambda b}(\lambda,T)$ is blackbody radiative intensity. Temperature-dependent reflectivity $\rho(\lambda,T)$ was measured by an accessory of Transmission-Reflection Dewar (Catalog No. DER-300, Harrick Scientific Products, Inc., America) mounting on the FT-IR spectrometer (VERTEX 80v, Bruker Co., Germany). The measured wavelength and temperature ranges are 2.5–25 μm and 97–373 K, respectively. A gold film was employed as a reference mirror to determine the reflectivity. It is inappropriate to the emissivity calculation at 97 K using Eq. (1) because the wavelength of maximum radiation energy λ_m=29.87 μm exceeds the measured wavelength regions of 2.5–25 μm on the basis of Wien's displacement law ($\lambda_m T = 2.8976 \times 10^{-3}$ m·K). In present work, therefore, the emissivity calculation is only considered in the temperature ranges of 123–373 K.

3. Results and discussion

The sputtering pressure difference in LSMO film growth creates a non uniform deposition rate as shown in Table 1. An interesting behavior is observed that the deposition rate increases firstly, and then decreases with the increase of sputtering pressure. It is understandable that a higher sputtering pressure tends to increase the frequency of Ar ions sputtering LSMO target, which in turn increase the deposition rate of film, while the deposition rate decreases in an overlarge pressure environment because it increases the collision between the mixed gas and the sputtered atoms, and then reduces the amounts of sputtered atoms arriving to substrate. The XRD patterns of several samples are shown in Fig. 1. The thickness of all the films is similar (900 nm). It can be seen that the annealed films show a perovskite character, which is in accord with the LSMO target. The non-annealed film in the inset of Fig. 1 exhibits an amorphous bread peak at 2θ=29°, which is a typical quartz glass state. The fact means that the LSMO film is difficult to crystallize with deposition at room temperature. A high temperature treatment therefore is necessary to obtain the desired perovskite structure through post

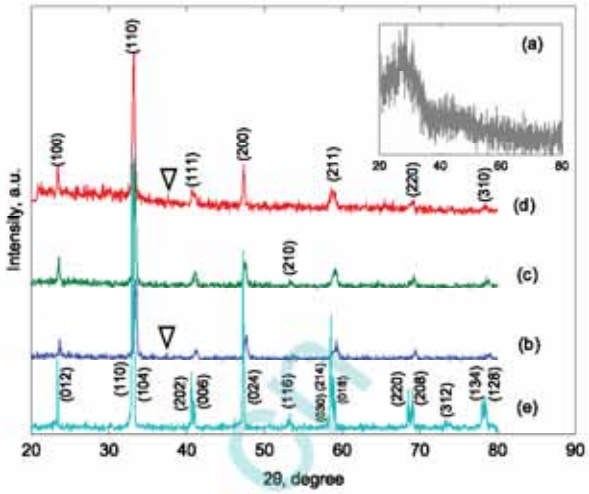

Fig. 1. XRD patterns of (a) LSMO film onto ACQ substrate without annealing, (b) LSMOACQ08, (c) LSMOACQ14, (d) LSMOACQ20, and (e) LSMO target.

annealing or in-situ heating substrate reported elsewhere [27]. For the films deposited on ACQ substrate, its diffraction peaks shift toward to lower angle direction (see the inset of Fig. 1) with the increase of sputtering pressure indicating that the lattice constant becomes larger, which is favor of enhancement of metal-insulator transition [28]. Compared to LSMO target, thin film has a relative larger diffraction angle owing to the easier strain relaxation in film [29]. In addition, Al diffraction peak at 2θ=38° can be detected in the annealed LSMO film as marked by symbol ∇, which is related to the use of Al layer.

SEM microstructure of LSMO film on ACQ substrate with different film thickness are shown in Fig. 2. The film with thickness about 0.9 μm is dense and crack-free, while the film with thickness about 1.52 μm exhibits a multi-crack character. The fact indicates that LSMO film deposition is difficult to obtain a thick film without defect by magnetron sputtering. In view of the instrument limit, the thick film with 1.52 μm thick is achieved through multiple pass sputter deposition. In other word, the thick film is composed of many single-pass films. If the film is too thick, the crack becomes more obvious due to existing strain. In addition, the crack formation is further exacerbated during the annealing process as a result of expanding with heat and contracting with cold. Consequently, the thick film will be not considered in present. A typical EDS spectrum of LSMO film on ACQ is presented in Fig. 2(c). Au element is from the Au layer used to enhance the image quality. Beside the detected Al element from Al layer and Si element from quartz substrate, the ratio of La:Sr:Mn:O is 0.66:0.41:1:2.6, which seems to be comparable with the stoichiometry ratios. However, the Sr concentration may be lower than the EDS results. As can be seen from the EDS spectra of LSMO film on ACQ in Fig. 2(c), it is difficult to discern the Sr and Si peak around 1.74 KeV due to their similar characteristic peak in EDS pattern. Thus, this means that the evaluated Sr concentration from EDS analysis may not be accurate enough. The similar result has been reported by other authors [30].

Fig. 3 shows the XPS patterns for LSMO film. From this global scan spectra it is clear that La, Sr, Mn, O, and C elements are present in the film. An enthetic S element is also observed due to the surface contaminant during test because our sample is impossible to contain the S element under the strict sputtering process. The S source may be from the SO_2 absorption experiment of other groups, which is performed simultaneously during our sample test. It was reported that the typical analysis depth is less than 10 nm for XPS, and it can arrive to 5 μm for EDS [31]. the information of Al layer and substrate are not observed in the XPS global scan pattern in our LSMO film. The carbon (C1s) region is from the atmospheric carbon contaminant and the other atmospheric hydrocarbons.

It can be noted that the La3*d* region in Fig. 3(b) shows a double-peak feature at 832 eV and 849 eV, which correspond to La3$d_{5/2}$ and La3$d_{3/2}$ core levels, respectively. The splitting energy both the core levels is equal to 17 eV. Meanwhile, an hump can be also observed for each of La3$d_{5/2}$ and La3$d_{3/2}$. The separation energy, for example, is 4 eV for the hump of La3$d_{5/2}$. Also, a split peak at 132 eV can be found in the Sr3*d* pattern (see Fig. 3(c)) due to the Sr3$d_{5/2}$ and Sr3$d_{3/2}$ core levels. The Mn2*p* region in Fig. 3 (d) shows two broad peaks at 640 and 651 eV, due to the Mn2$p_{1/2}$ and Mn2$p_{3/2}$ core levels, respectively. The measured photoelectron spectra of O1*s* in Fig. 3(e) shows the O1*s* peak at 528 eV and another shoulder peak at 530 eV, indicating two types of oxygen present on the sample surface. The former is assigned to O^{2-} ion of the metal oxide [32], while the broad shoulder peak is probably due to a superposition of two peaks between the absorbed hydroxide on sample surface and the SrO [21]. According to the statistics of atom % shown in the embedded table of Fig. 3, the ratios of La/Mn, and Sr/Mn in LSMO film surface can be obtained, which is 0.5 and 1.38, respectively. The ratio of La/Mn is close to that of EDS result, while it is larger than that of EDS result for the Sr/Mn. The high ratio of Sr/Mn is similar with previous observations on the film fabricated by reactive pulsed laser deposition [21]. In fact, it is difficult to ensure the concentration of La, Sr, Mn, and O elements from XPS analysis in LSMO film in agreement with that from EDS analysis.

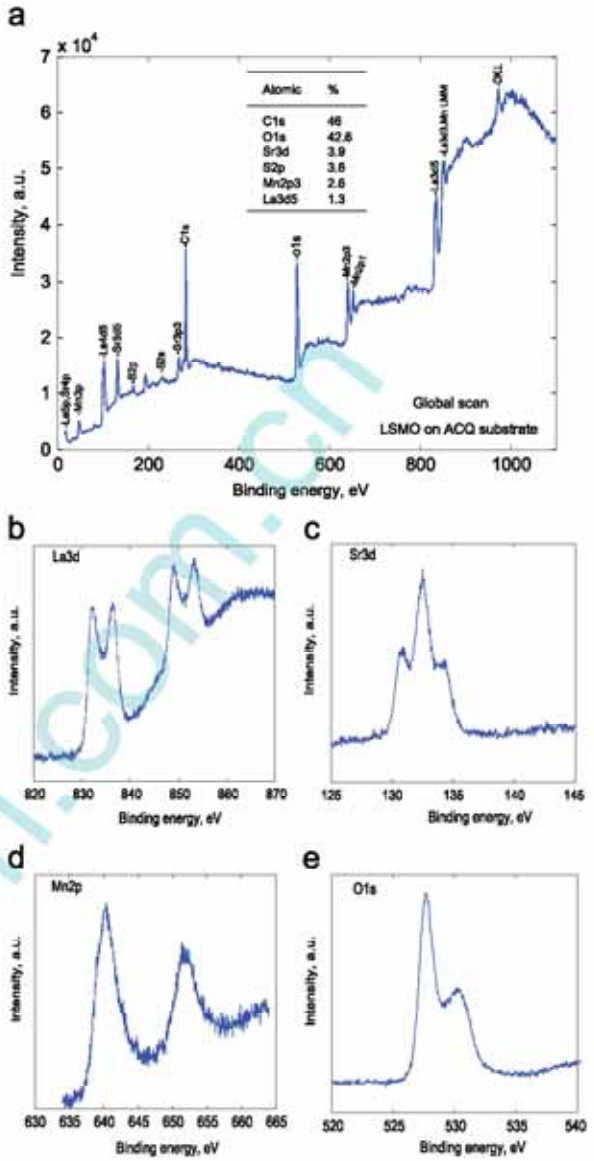

Fig. 3. XPS spectra of (a) LSMO film on ACQ substrate, (b) La3d, (c) Sr3d, (d) Mn2p, and (e) O1s.

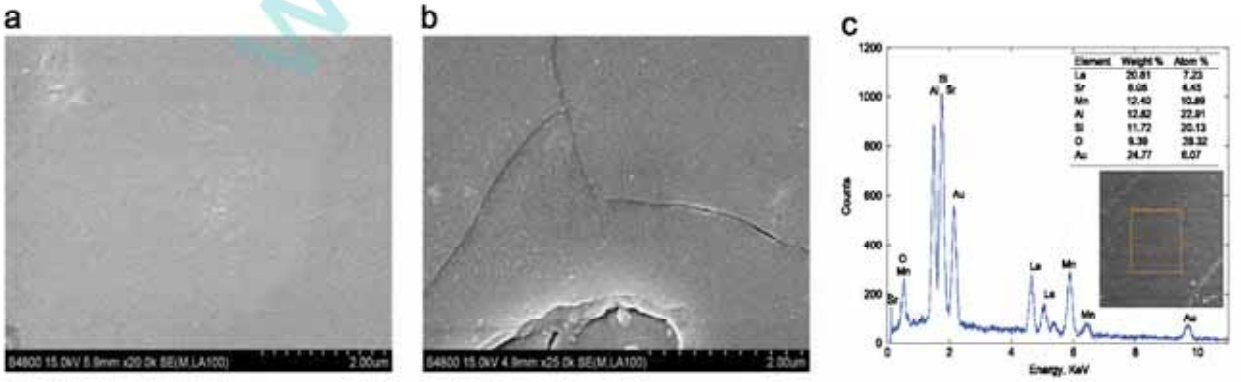

Fig. 2. Surface micrographs of LSMO film on ACQ substrate with film thickness (a) 0.9 μm and (b) 1.52 μm, and (c) EDS pattern.

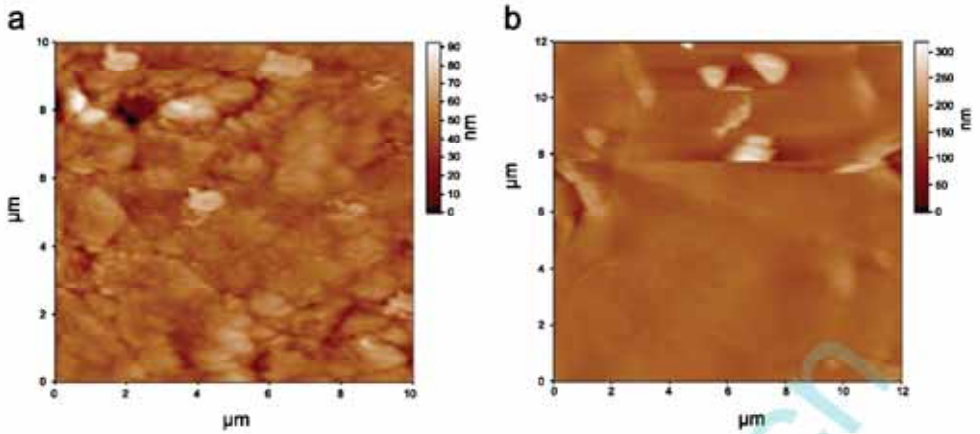

Fig. 4. AFM images of LSMO film on ACQ substrate with film thickness (a) 0.9 μm and (b) 1.52 μm.

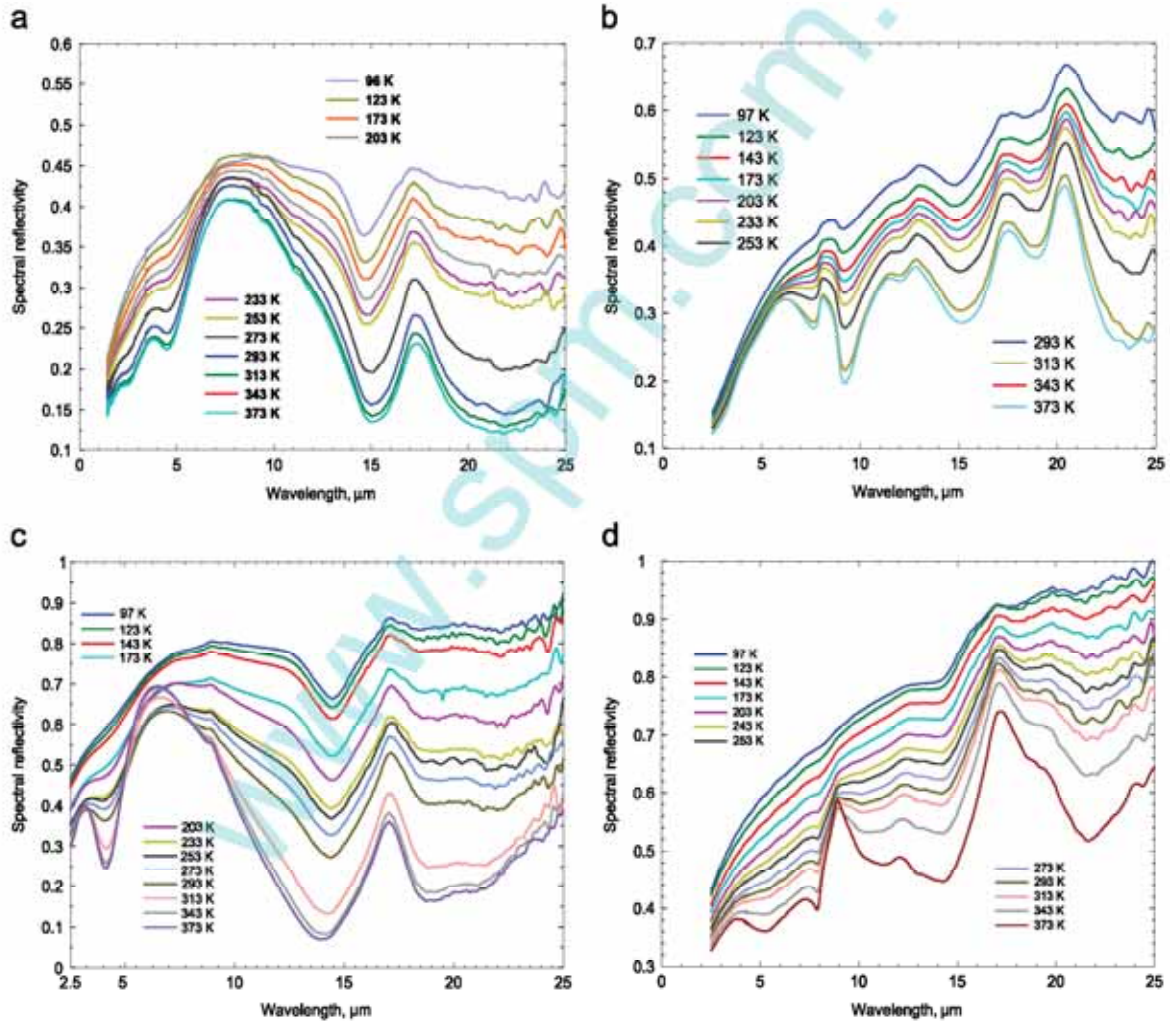

Fig. 5. Reflectivity of LSMO film at different working pressure for (a) 0.5 Pa, (b) 0.8 Pa, (c) 1.4 Pa, and (d) 2.0 Pa.

AFM images of LSMO film with different film thickness are displayed in Fig. 4. It is noted that the surface morphology of the films change with thickness due to the change in the growth mode, which in turn causes a variation in surface roughness. The root mean square roughness is estimated to be 6.29 nm and 45.6 nm for the film with thickness 0.9 μm and 1.52 μm respectively, revealing a relative smooth LSMO film surface.

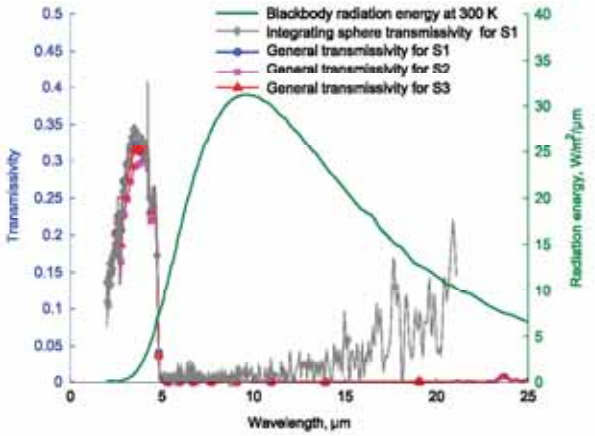

Fig. 6. Room temperature transmissivity of LSMO film at 1.4 Pa sputtering pressure. Transmissivity consistency is verified by measuring three samples (S1, S2, and S3) from the same growth condition.

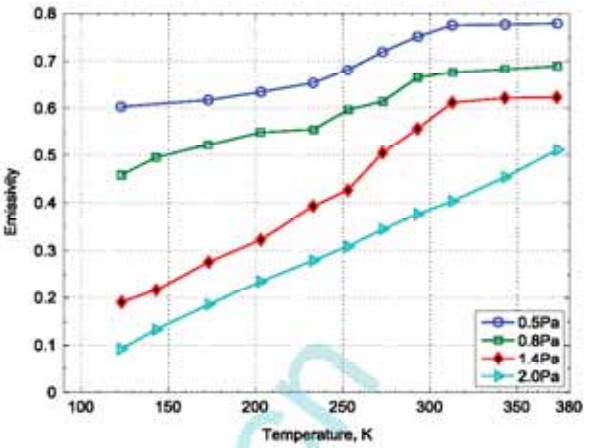

Fig. 7. Emissivity of LSMO film at different sputtering pressure.

Fig. 5 shows the measured reflectivity of LSMO film in the temperature range of 97–373 K. It is noted that the reflectivity of film decreases with increasing temperature. A sharp infrared peak at the wavelength of 17 μm under different test temperature can be observed, which dues to the transverse optical phonons. In theory, there are three strong transverse optical phonon peaks in perovskite sample [33–35]. The other two phonon peaks occur at 30 μm and 60 μm, corresponding to Mn-O-Mn bending mode, and La-site external mode, respectively. In view of the limited spectral range of spectrometer, we only observed the optical phonon peak corresponding to Mn-O stretching vibration in our samples. The phonon peak toward the low temperature 97 K is still sharp comparing with that of LSMO bulk material, which has been reported in the previous works [5,35]. The fact suggests that LSMO film is "more nonmetallic" than its bulk counterpart at low temperature zones. For the LSMO bulk material, the lower temperature is, the smoother peak at 17 μm becomes. The phenomenon has been explained by an dielectric screening effect [33,36]. Namely, the electron activity in bulk material is heighten under a lower temperature. Therefore, it is considered that the contribution of optical phonon in LSMO film is still dominant under the lower temperature, which leads to LSMO film exhibiting more nonmetallic features. The sharp peaks under low temperature zones seem to be common in manganite film as reported by these authors [19,20]. With the increase of temperature, there are still notable broad peaks appearing in the wavelength range of 5–10 μm in present films. The fact reveals that the film samples become more prone to insulator at high temperature. Similar features have been observed by pervious authors in both single crystalline [35,37] and thin film manganites [19,21,38,39,28]. For the single crystalline samples $La_{1-x}Sr_xMnO_3$ ($x=0.1$, 0.175, and 0.3), it has been observed that the insulator phase sample for $x=0.1$ also shows a broad peak at the same wavelength range, while the peak disappears for the sample $x=0.175$ and 0.3 [35]. Likewise, the single crystal sample $Nd_{0.7}Sr_{0.3}MnO_3$ also exhibits a broad peak above 200 K at the same region, which is suggested to come from the optical transitions between electronic levels [37]. Hartinger et al. [38] reported that the broad peaks are related to the large polarons excitation in $La_{2/3}Sr_{1/3}MnO_3$ thin film. Other possibilities may be exist such as oxygen deficiency, inhomogeneity, and disorder. Since the oxygen content increases with the rise of sputtering pressure resulting in the reduction of oxygen deficiency in film, the broad peak exhibits an obvious diminution at high sputtering pressure, epically 2.0 Pa.

In order detect the transmission properties of LSMO film, the integrating sphere method using the integrating sphere accessory (A-562-G, Bruker Optik GmbH) and general transmissivity method are used. The accessory is possible to transmission assessment, although there is a high signal loss as shown in instruction manual. The integrating sphere transmissivity includes the light transmission and scatter of the measured sample, which is collected inside the integrating sphere and detected by detector. It can be found from Fig. 6 the integrating sphere transmissivity shows a high signal loss especially beyond the wavelength of 15 μm. The transmissivity of three samples (S1, S2, and S3) from the same growth condition (1.4 Pa sputtering pressure) shows almost coincident results as shown in Fig. 6. It can be seen that the samples are opaque except for the low transmissivity less than 0.35 around the wavelength of 3.6 μm. According to the blackbody radiation spectra at 300 K as shown in Fig. 6, which is determined by Planck's spectral distribution of emissive power, the proportion of emissive energy is small below 5 μm wavelength. The emissivity calculation in present work therefore ignores the transmissivity of the samples.

Infrared emissivity of LSMO film on ACQ substrate is obtained by integrating its reflectivity spectra [11]. The results are shown in Fig. 7. It can be observed that the LSMO films show different emissivity variation with the change of sputtering pressure. The emissivity of these films increases with increasing temperature and undergoes a sharp variation except the film grown at 2.0 Pa. Film grown at 0.5 Pa sputtering pressure has a high emissivity in the whole temperature range. This is caused by the low pressure sputtering process that contains less oxygen due

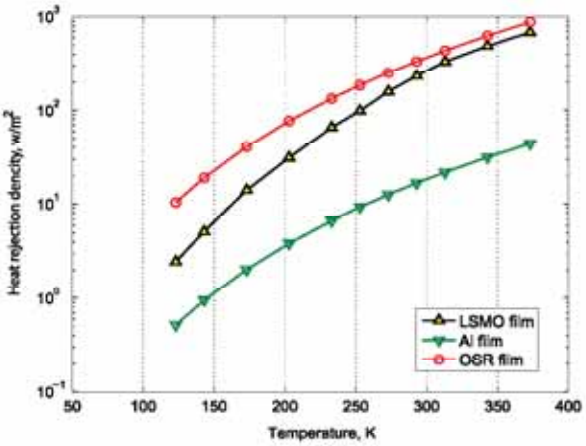

Fig. 8. Emissivity effect on the heat rejection capacity due to the temperature fluctuation.

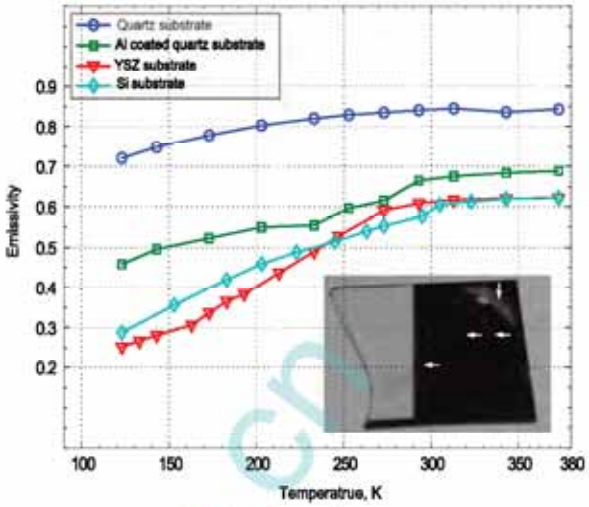

Fig. 9. Emissivity of LSMO film with different substrate. The inset is a broken film sample deposited on quartz and the peeled portions are marked by arrows.

to the small amount of oxygen atoms in the deposition environment. Moreover, the low bombardment frequency resulting from the low pressure is conducive to form defect in the films. The formed defect such as oxygen defect is detrimental to break the hoping bridge of double-exchange presented by Zener [40], which reduces the conduction activity of electron. With the increase of pressure up to 2.0 Pa, the variation of oxygen concentration leads to hole doping through an augment of the Mn^{4+}/Mn^{3+}. In addition, the oxygen incorporation within columns or grains of the film structure can also be suggested to strengthen the metal-insulator transition toward to a higher temperature. Therefore, these contributions lead to a decrease of the emissivity of film in addition to an increase of metal-insulator transition temperature reported by Sahu [41]. Temperature-dependent emissivity of film deposited at 2.0 Pa is smaller than that of the other film samples and no drastic change can be observed in the entire temperature range as the film is in the metallic state in the temperature region like its bulk counterpart reported in reference [1]. Large emissivity at higher temperature is necessary to enhance the ability of heat dissipation in spacecraft application and small emissivity at lower temperature is still important to prevent the heat loss from the inside of spacecraft. Thereby, the emissivity variation properties of the film deposited at 1.4 Pa are attractive in spacecraft application.

Spacecraft thermal control materials are described by their heat rejection capacity. If the thermochromic film is deposited onto the spacecraft skin without suffering solar radiation, its heat rejection capacity $\dot{Q}$ can be represented by $\dot{Q}/A = \dot{q} = \epsilon\sigma(T_s^4 - T_b^4)$. Here, σ is the Stefan–Boltzmann constant(5.67×10^{-8} W/m$^2 \cdot$ K^4), A is the thermal control surface area, $\dot{q}$ is the heat rejection density, T_s is the thermal control surface temperature, T_b is the space background temperature(4 K), ϵ is the emissivity of the thermal control material. This is only a simplified model to account for a thermal control application for thermochromic film. Here, we calculated the heat rejection density $\dot{q}$ of three thermal control materials (Aluminium, OSR, and LSMO film deposited at 1.4 Pa, respectively.) to evaluate their application performance. The calculated results are shown in Fig. 8. If the temperature fluctuation of spacecraft surface is required in the range of 250–300 K, one expects a large enough heat rejection density above 300 K and a small enough heat rejection density or a suitable heating below 250 K. It can be found that OSR film ($\epsilon = 0.8$) and Al film ($\epsilon = 0.04$) are the expected thermal control materials above 300 K and below 250 K, respectively. Unfortunately, the usage of OSR requires an auxiliary heater when the temperature is low to 250 K and the usage of Al film needs an auxiliary cooler above 300 K. This means an additional power consumption and moving parts are required. However, the usage of LSMO film can reduce or avoid heater requirement because of its lower heat loss than that of OSR film below 250 K and comparable heat rejection capacity above 300 K. By comparison, the thermal control performance of LSMO film is obvious.

Comparisons are given for the emissivity of LSMO film deposited at different substrate in Fig. 9. Considering the effect of substrate on the emissivity of LSMO film, it can be found that the largest emissivity is obtained for the film on quartz substrate. Its emissivity value is larger than that of literature results in the entire temperature range [28], probably because of the influence of substrate. The adherence strength of the film on the quartz is low. The inset in Fig. 9 shows a broke film sample deposited on quartz after standing for several days in air. Therefore, the contribution of substrate can be reflected in the emissivity curve. The metal-insulator transition in manganite films is extremely related to the growth condition and substrate characteristics which influence the microstructures of the manganite films, and then their optical, thermal, electrical, and magnetic properties [21,42,43]. The transition temperature point estimated from the emissivity-temperature curves is different in our films which apparently accounts for this. The emissivity of the film on ACQ substrate is relative larger than that of the film on YSZ and Si substrate. Difference in the emissivity value may be due to the interface problems and change in the strain behaviors of the film and substrate. The presence of inhomogeneity, mostly existing at the interface, also

significantly influences the thermal radiative properties. There may be exist other possibilities such as oxygen non-stoichiometry in films. These factors are important to device design and application.

4. Conclusion

Thermochromic films are prepared on different substrates by magnetron sputtering technique. Ex-situ annealing in oxygen atmosphere improves the film crystallization and oxygen balance. Surface morphology indicated that crack-free thick films is difficult to be deposited by sputtering. XRD analysis showed that the films exhibit the characteristics of perovskite structure. Reflectivity spectra show that the oxygen deficiency is related to the sputtering pressure. Sputtering pressure effect on thermochromic film properties is investigated. Emissivity of the film is large at high temperature and it decreases sharply upon cooling. Difference in emissivity is not only dependent on the sputtering pressure but also strain behavior of film and substrate. Film deposited on ACQ substrate with 1.4 Pa sputtering pressure shows good thermochromic properties, which is comparable with existing OSR film in spacecraft thermal control.

Acknowledgments

This work is sponsored by the National Science Foundation of China (Grant no. 51406086), the Natural Science Foundation of Jiangsu Province (No. BK20140783), the 2014 Zijin Intelligent Program of Nanjing University of Science and Technology.

Appendix A. Supplementary data

Supplementary data associated with this article can be found in the online version at http://dx.doi.org/10.1016/j.actaastro.2016.01.001.

References

[1] K. Shimazaki, S. Tachikawa, A. Ohnishi, Y. Nagasaka, Radiative and optical properties of $La_{1-x}Sr_xMnO_3$ ($0<x<0.4$) in the vicinity of metal-insulator transition temperatures from 173 to 413 K, Int. J. Thermophys. 22 (2001) 1549–1561.

[2] K. Shimazaki, S. Tachikawa, A. Ohnishi, Y. Nagasaka, Temperature dependence of total hemispherical emittance in perovskite-type manganese oxides, $La_{1-x}Sr_xMnO_3$, High Temp.-High Press. 33 (2001) 525–531.

[3] S. Tachikawa, A. Ohnishi, Y. Shimakawa, A. Ochi, A. Okamoto, Y. Nakamura, Development of a variable emittance radiator based on a perovskite manganese oxide, J. Thermophys. Heat Transf. 17 (2003) 264–268.

[4] A. Ochi, T. Mori, Y. Shimakawa, Y. Kubo, A. Okamoto, Y. Nakamura, S. Tachikawa, A. Ohnishi, K. Shimazaki, Variable thermal emittance radiator using metal-insulator phase transition in $La_{1-x}Sr_xMnO_3$, Jpn. J. Appl. Phys. 41 (2002) 7263–7265.

[5] D. Fan, Q. Li, Y. Xuan, H. Tan, J. Fang, Temperature-dependent infrared properties of Ca doped $(La,Sr)MnO_3$ compositions with potential thermal control application, Appl. Therm. Eng. 51 (2013) 255–261.

[6] S. Tachikawa, A. Ohnishi, K. Shimazaki, A. Okamoto, Y. Nakamura, Y. Shimakawa, T. Manako, T. Mori, A. Ochi, Development of a variable emittance radiator, in: 29th International Conference on Environment Systems, SAE Technical Paper Series, Denver, Colorado, 1999, pp. 1–5.

[7] L. Li, C. Wang, Y. Shen, Q. Shen, L. Zhang, Influence of annealing on structure and thermochromic property of spark plasma sintered $La_{1-x}Sr_xMnO_3$, J. Mater. Sci.: Mater. Electron. 26 (2015) 2508–2513.

[8] K. Shimazaki, A. Ohnishi, Y. Nagasaka, Development of spectral selective multilayer film for a variable emittance device and its radiation properties measurements, Int. J. Thermophys. 24 (2003) 757–769.

[9] K. Shimazaki, A. Ohnishi, Y. Nagasaka, Computational design of solar reflection and far-infrared transmission films for a variable emittance device, Appl. Opt. 42 (2003) 1360–1366.

[10] D. Fan, Q. Li, Y. Xuan, Tailoring the solar absorptivity of thermochromic material $La_{0.7}Ca_{0.2}Sr_{0.1}MnO_3$, J. Quant. Spectrosc. Radiat. Transf. 112 (2011) 2794–2800.

[11] D. Fan, Q. Li, Y. Xuan, H. Tan, J. Fang, Radiative properties of thermochromic material with solar reflection films, Sol. Energy Mater. Sol. Cells 112 (2013) 52–56.

[12] D. Fan, Q. Li, Y. Xuan, H. Tan, Degradation of thermal radiative properties of variable emissivity device based on manganese oxides in simulated space environment, Int. J. Therm. Sci. 71 (2013) 258–263.

[13] S. Tachikawa, K. Shimazaki, A. Ohnishi, H. Hirosawa, Y. Shimakawa, A. Ochi, A. Okamoto, Y. Nakamura, Smart radiation device based on a perovskite manganese oxide, in: Proceedings of the 9th International Symposium on Materials in a Space Environment, Noordwijk, The Netherlands, 2003, pp. 41–47.

[14] S. Tachikawa, A. Ohnishi, Y. Nakamura, A. Okamoto, Ground tests and in-orbit performance of variable emittance device based on manganese oxide, Jpn. Soc. Aeronaut. Space Sci. 55 (2007) 367–372.

[15] J. Huang, Y. Xuan, Q. Li, Investigation on emissive properties of peroskite-type oxide LSMO with grating surface, Sci. China Technol. Sci. 54 (2011) 220–225.

[16] J. Fang, Y. Xuan, Q. Li, D. Fan, J. Huang, Investigation on the coupling effect of thermochromism and microstructure on spectral properties of structured surfaces, Appl. Surf. Sci. 258 (2012) 7140–7145.

[17] J. Huang, Y. Xuan, Q. Li, Perovskite-type oxide films combined with gratings for reduction of material consumption and improvement of thermochromism property, J. Quant. Spectrosc. Radiat. Transf. 112 (2011) 2592–2599.

[18] Y. Xuan, An overview of micro/nanoscaled thermal radiation and its applications, Photonics Nanostructures-Fundam. Appl. 12 (2014) 93–113.

[19] Y. Shimakawa, T. Yoshitake, Y. Kubo, T. Machida, K. Shinagawa, A. Okamoto, Y. Nakamura, A. Ochi, S. Tachikawa, A. Ohnishi, A variable-emittance radiator based on a metal-insulator transition of $(La,Sr)MnO_3$ thin films, Appl. Phys. Lett. 80 (2002) 4864–4866.

[20] Q. Li, D. Fan, Y. Xuan, Thermal radiative properties of plasma sprayed thermochromic coating, J. Alloys Compd. 583 (2014) 516–522.

[21] M. Soltani, M. Chaker, X.X. Jiang, D. Nikanpour, J. Margot, Thermochromic $La_{1-x}Sr_xMnO_3$ ($x=0.1$, 0.175, and 0.3) smart coatings grown by reactive pulsed laser deposition, J. Vacuum Sci. Technol. A24 (2006) 1518.

[22] D. Nikanpour, X.X. Jiang, S. Genaron, G. Wang, An autonomous variable emittance thermal radiator for small & microsat temperature control, in: 4th Symposium of Small Satellites Systems and Services, ESA, Noordwijk, The Netherlands, 2008, pp. 46. SP–660.

[23] C. Wu, J. Qiu, Y. He, Relevancy of phase separation between electrical and thermal properties in $La_{0.8}Sr_{0.2}MnO_3$ thin films, Phys. B: Condens. Matter 406 (2011) 1886–1889.

[24] C.H. Lee, D.R. Kim, X. Zheng, Transfer printing methods for flexible thin film solar cells: basic concepts and working principles, ACS Nano 8 (2014) 8746–8756.

[25] C.H. Lee, D.R. Kim, I.S. Cho, N. William, Q. Wang, X. Zheng, Peel-and-stick: fabricating thin film solar cell on universal substrates, Sci. Rep. 2 (2012).

[26] ECSS-Q-70-09A. ESA space product assurance—measurements of thermo-optical properties of thermal control materials, 2003.

[27] D.R. Sahu, The properties of $La_{0.7}Sr_{0.3}MnO_3$ films prepared by DC magnetron sputtering using nanosized powder compacted target: effect of substrate temperature, Appl. Surf. Sci. 255 (2008) 1870–1873.

[28] C. Wu, J. Qiu, J. Wang, M. Xu, L. Wang, Thermochromic property of $La_{0.8}Sr_{0.2}MnO_3$ thin film material sputtered on quartz glass, J. Alloys Compd. 506 (2010) L22–L24.

[29] P. Siwach, H. Singh, O. Srivastava, Influence of strain relaxation on magnetotransport properties of epitaxial $La_{0.7}Ca_{0.3}MnO_3$ films, J. Phys.: Condens. Matter 18 (2006) 9783.

[30] J. Wang, Study on preparation and phase transition property of $La_{1-x}Sr_xMnO_3$ thin films (In chinese) (Master's thesis), Lanzhou University, 2012.
[31] Q. Chen, K. Rezwan, D. Armitage, S. Nazhat, A. Boccaccini, The surface functionalization of 45s5 bioglass®-based glass-ceramic scaffolds and its impact on bioactivity, J. Mater. Sci.: Mater. Med. 17 (2006) 979–987.
[32] Q.-H. Wu, M. Liu, W. Jaegermann, X-ray photoelectron spectroscopy of $La_{0.5}Sr_{0.5}MnO_3$, J. Mater. Sci.: Mater. Med. 59 (2006) 1980–1983.
[33] Y. Okimoto, T. Katsufuji, T. Ishikawa, A. Urushibara, T. Arima, Y. Tokura, Anomalous variation of optical spectra with spin polarization in double-exchange ferromagnet $La_{1-x}Sr_xMnO_3$, Phys. Rev. Lett. 75 (1995) 109–112.
[34] K.H. Kim, J.Y. Gu, H.S. Choi, G.W. Park, T.W. Noh, Frequency shifts of the internal phonon modes in $La_{0.7}Ca_{0.3}MnO_3$, Phys. Rev. Lett. 77 (1996) 1877–1880.
[35] Y. Okimoto, T. Katsufuji, T. Ishikawa, T. Arima, Y. Tokura, Variation of electronic structure in $La_{1-x}Sr_xMnO_3$ ($0 < x < 0.3$) as investigated by optical conductivity spectra, Phys. Rev. B 55 (1997) 4206–4214.
[36] G.D. Marzi, Z.V. Popović, A. Cantarero, Z. Dohčević-Mitrović, N. Paunović, J. Bok, F. Sapiña, Effect of a-site and b-site substitution on the infrared reflectivity spectra of $La_{1-y}A_yMn_{1-x}B_xO_3$ (A=Ba,Sr; B=Cu, Zn, Sc; $0 < y \leq 0.3$; $0 \leq x \leq 0.1$) manganites, Phys. Rev. B 68 (2003) 064302.
[37] H. Lee, J. Jung, Y. Lee, J. Ahn, T. Noh, K. Kim, S. Cheong, Optical properties of a $Nd_{0.7}Sr_{0.3}MnO_3$ single crystal, Phys. Rev. B 60 (1999) 5251.
[38] C. Hartinger, F. Mayr, J. Deisenhofer, A. Loidl, T. Kopp, Large and small polaron excitations in $La_{2/3}(Sr/Ca)_{1/3}MnO_3$ films, Phys. Rev. B 69 (2004) 100403.
[39] S. Jiang, X. Ma, G. Wang, G. Tang, Z. Wang, Z. Zhou, Characteristics of $La_{0.7}Sr_{0.3}MnO_{3-\delta}$ films treated by oxygen plasma immersion ion implantation, Surf. Coat. Technol. 229 (2013) 76–79.
[40] C. Zener, Interaction between the d-shells in the transition metals. II. ferromagnetic compounds of manganese with perovskite structure, Phys. Rev. 82 (1951) 403–405.
[41] D.R. Sahu, $La_{0.7}Sr_{0.3}MnO_3$ film prepared by dc sputtering on silicon substrate: effect of working pressure, J. Phys. Chem. Solids 73 (2012) 622–625.
[42] A. Urushibara, Y. Moritomo, T. Arima, A. Asamitsu, G. Kido, Y. Tokura, Insulator-metal transition and giant magnetoresistance in $La_{1-x}Sr_xMnO_3$, Phys. Rev. B 51 (1995) 14103.
[43] S. Khartsev, P. Johnsson, A.M. Grishin, Colossal magnetoresistance in ultrathin epitaxial $La_{0.7}Sr_{0.25}MnO_3$ films, J. Appl. Phys. 87 (2000) 2394–2399.